

Slowing-down of non-equilibrium concentration fluctuations in confinement

Cédric Giraudet¹, Henri Bataller¹, Yifei Sun², Aleksandar Donev², José Maria Ortiz de Zárate³ and Fabrizio Croccolo¹

¹*Laboratoire des Fluides Complexes et leurs Réservoirs,*

Université de Pau et des Pays de l'Adour, 64600 Anglet, France

²*Courant Institute of Mathematical Sciences, New York University, New York, NY 10012, USA and*

³*Departamento de Física Aplicada I, Universidad Complutense, 28040 Madrid, Spain*

(Dated: October 27, 2022)

Fluctuations in a fluid are strongly affected by the presence of a macroscopic gradient making them long-ranged and enhancing their amplitude. While small-scale fluctuations exhibit diffusive lifetimes, larger-scales fluctuations live shorter because of gravity, as theoretically and experimentally well-known. We report experimental evidence of a dramatic slowing-down for fluctuations larger than a size dictated by the extent of the system in the direction of the gradient. We find diffusive behaviour for strongly-confined fluctuations but with a diffusion coefficient that depends strongly on the solutal Rayleigh number. Results from dynamic shadowgraph experiments are complemented by theoretical calculations and numerical simulations based on fluctuating hydrodynamics, and excellent agreement is found. Our work indicates that the study of the dynamics of non-equilibrium fluctuations allows to probe and measure the competition of physical processes such as diffusion, buoyancy and confinement.

PACS numbers: 05.40.-a, 05.70.Ln, 47.11.-j, 42.30.Va

It is well established that fluctuations are long-ranged in systems out of equilibrium [1], even far from critical points where the long-range behaviour is observed also in equilibrium conditions [2]. In a binary fluid mixture subjected to a stabilizing temperature or concentration gradient, the coupling between the spontaneous velocity fluctuations and the macroscopic gradient results in giant concentration fluctuations in the quiescent state [1, 3]. Gravity is known to quench the magnitude of fluctuations with length scales larger than a characteristic size $2\pi/q_s^*$ related to the dimensionless solutal Rayleigh number Ra_s of the system [3, 4], defined by

$$Ra_s = \frac{\beta_s g \nabla c L^4}{\nu D}; \quad -Ra_s = (q_s^* L)^4, \quad (1)$$

where $\beta_s = \rho^{-1}(\partial\rho/\partial c)$ is the solutal expansion coefficient, ρ the fluid density, g the gravity acceleration, c the concentration of the denser component of the fluid mixture, ∇c the modulus of the concentration gradient, D the mass diffusion coefficient, ν the kinematic viscosity, and q_s^* a characteristic solutal wave vector. Boundaries are known to suppress fluctuations larger than the confinement length L in the direction of the gradient [1, 5]. Gravity is also known to accelerate the dynamics of the fluctuations for wavenumbers smaller than q_s^* via buoyancy effects, leading to non-diffusive decay of large-scale fluctuations [6].

In this Letter we show, through a combination of experimental measurements, theoretical calculations, and numerical simulations, that confinement leads to a dramatic slowdown of fluctuations for wavenumbers below $q_b \cong 5/L$, restoring diffusive scaling of the relaxation rate, but with a diffusion coefficient $(1 - Ra_s/720)$ times larger than the Fickian diffusion coefficient (for $Ra_s < 720$, which is the convective threshold for this problem

[7]). For the range of Ra_s investigated in this paper, $q_b < q_s^*$, leading to a rich and diverse dynamical behaviour depending on the wavenumber of the fluctuations.

We experimentally investigate the dynamics of concentration non-equilibrium fluctuations (c-NEFs) in the presence of a vertical concentration gradient in a binary liquid mixture by means of dynamic shadowgraph [6, 8]. The dynamics can be characterized in terms of the Intermediate Scattering Function (ISF or, equivalently, normalized time correlation function) $f(q, t)$, with $f(q, 0) = 1$. At first approximation the ISF can be modeled by a single exponential decay with decay time $\tau(q)$ depending on the analysed wave vector q . Available theories accounting for the simultaneous presence of diffusion (d) and gravity (g) [9, 10], but not for confinement, predict for a stable ($Ra_s < 0$) configuration:

$$\left. \frac{\tau(\tilde{q})}{\tau_s} \right|_{d+g} = \frac{1}{\tilde{q}^2 \left(1 - \frac{Ra_s}{\tilde{q}^4}\right)}, \quad (2)$$

where the wave vector is expressed in its dimensionless form $\tilde{q} = qL$ and $\tau_s = L^2/D$ is the typical solutal time it takes diffusion to traverse the thickness of the sample. Equation (2) implies different behaviours for the decay times of small-scale and large-scale fluctuations,

$$\left. \frac{\tau(\tilde{q})}{\tau_s} \right|_d = \frac{1}{\tilde{q}^2} \quad \text{for } \tilde{q} \gg \tilde{q}_s^*, \quad (3)$$

and

$$\left. \frac{\tau(\tilde{q})}{\tau_s} \right|_g = -\frac{\tilde{q}^2}{Ra_s} \quad \text{for } \tilde{q} \ll \tilde{q}_s^*, \quad (4)$$

suggesting that the fluctuation decay time has a maximum (clearly visible in Fig.1) at the solutal characteristic

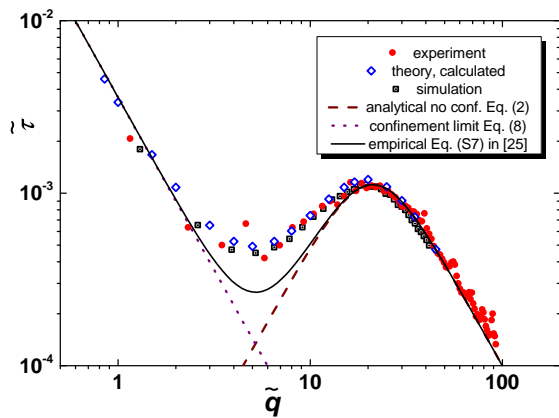


FIG. 1. (color online) Dimensionless decay times: Log-log plot of the (effective) dimensionless decay times $\tilde{\tau} = \tau/\tau_s$ as a function of dimensionless wave number $\tilde{q} = qL$ for $Ra_s = -2 \cdot 10^5$. The brown dashed line depicts the analytical solution provided by Eq.(2) which takes into account only the effect of gravity and diffusion, while the purple dotted line is for the confinement limit expressed by Eq.(8). Filled red circles are experimental data obtained on a tetralin-n-dodecane sample. Open blue diamonds are the result of theoretical calculations based on the FHD model. Open-dotted black squares are obtained by numerical simulations on a sample with analogous parameters. For dimensionless wave numbers $\tilde{q} \lesssim 5.2$ a slowing down is clear, and is due to confinement, as evidenced by the agreement among experiment, simulation and theory. The continuous black line shows the empirical Eq.(S7) in [25].

wave vector \tilde{q}_s^* , which identifies the most persistent fluctuation in the system.

The behaviour predicted by Eq.(2) has been experimentally verified in a number of experiments on c-NEFs related to a pure concentration gradient (isothermal mass diffusion) [6, 11, 12] or to a concentration gradient induced by the Soret effect [8, 13]. Note that Eq. (4) implies a non-diffusive behaviour with fluctuations of larger length scale decaying faster, which is a rather non-intuitive result [6] if extrapolated to $\tilde{q} \rightarrow 0$.

To clarify the small wavenumber behaviour of c-NEFs, here we revisit the experiments with an experimental setup that contains a state-of-the-art CCD detector, allowing us to observe fluctuations at wave numbers down to $q_{\min} = 8.89 \text{ cm}^{-1}$. We applied a stabilizing temperature difference $\Delta T = 20 \text{ K}$ (with an average temperature of 298 K) to a horizontal layer of tetralin and n-dodecane at 50% weight fraction of vertical thickness $L = 1.3 \text{ mm}$ and lateral extent $R = 13.0 \text{ mm}$. Details of the thermal gradient cell can be found elsewhere [8, 14]. Here we mention that the sample thickness can be varied by using different plastic spacers and sealing O-rings.

The rapid imposition of a temperature difference by heating the fluid mixture from above results in the establishment of a linear temperature profile across the sample in a thermal time $\tau_T = L^2/\kappa$, where κ is the

thermal diffusivity. Due to the much smaller value of the mass diffusion coefficient, a nearly linear concentration profile is generated by means of the Soret effect [15, 16] in a much larger solutal or mass diffusion time τ_s . Since the investigated mixture has a positive separation ratio ψ , both the temperature and the concentration profile result in a stabilizing density profile and the only variations in the temperature and concentrations are due to intrinsic fluctuations.

Shadowgraphy [17–20] allows the recording of images whose intensities contain a mapping of the sample refractive index fluctuations, over space and time, averaged along the direction of the gradient. This is quite similar to conventional Dynamic Light Scattering, but with a shadowgraph we can access smaller wave vectors, exactly were gravity and confinement effects are expected to strongly affect the c-NEFs. Shadowgraph image analysis is performed by the Differential Dynamic Algorithm [6, 8, 11, 12, 21, 22], where one directly computes the so-called structure function:

$$C(q, t) = \langle |\Delta i_m(\mathbf{q}, \Delta t)|^2 \rangle_{t, |\mathbf{q}|=q} = \langle |i(\mathbf{q}, t) - i(\mathbf{q}, t + \Delta t)|^2 \rangle_{t, |\mathbf{q}|=q}, \quad (5)$$

with $i(\mathbf{q}, t) = \mathcal{F}[I(\mathbf{x}, t)/\langle I(\mathbf{x}, t) \rangle_{\mathbf{x}}]$ the 2D-Fourier transform of a normalized image $I(\mathbf{x}, t)$. The structure function is related to the ISF via [6, 8, 11, 21]:

$$C(q, t) = 2A\{T(q)S(q)[1 - f(q, \Delta t)] + B(q)\}, \quad (6)$$

where $T(q)$ is the optical transfer function of the instrument, A an intensity pre-factor, and $B(q)$ a background including all the phenomena with time-correlation functions that decay faster than the CCD frame rate, such as contributions due to shot noise and temperature fluctuations. $S(q)$ in Eq. (6) represents the static intensity of the c-NEFs as a function of the wavenumber.

From the $f(q, t)$ evaluated via Eqs. (5)-(6), we obtained the experimental effective decay times of c-NEFs reported in Fig. 1. The sample thermophysical properties [23] result in a solutal Rayleigh number $Ra_s = -2 \cdot 10^5$. Figure 1 shows that for essentially all wave vectors smaller than the solutal characteristic wave vector $\tilde{q}_s^* = \sqrt[3]{-Ra_s} \cong 21$, the measured decay time departs from the theoretical description of Eq. (2). Quite unexpectedly, as the wave vector is decreased the decay time presents a minimum for a dimensionless wave vector $\tilde{q}_b \cong 5$ and for smaller wave vectors it decreases in a manner consistent with a diffusive decay $\tilde{\tau} \propto \tilde{q}^{-2}$.

In order to interpret these experimental findings we use a Fluctuating Hydrodynamics (FHD) model [5] that incorporates gravity and confinement. The intensity $S(q)$ of c-NEFs implied by this model was analyzed in a previous publication [5]. We deduce here that, from the model [5], the dynamic structure factor $S(q, t)$ of the c-

NEFs will be expressed as:

$$S(q, t) = S(q)f(q, t) = \sum_{N=1}^{\infty} A_N(q) \exp \left[-\frac{t}{\tau_N(q)} \right], \quad (7)$$

see [25] for further details. The decay times in Eq.(7) are the inverse of the eigenvalues $\Gamma_N(q) = 1/\tau_N(q)$ solving Eq. (43) in Ref. [5]. The amplitudes A_N are analytically related to Γ_N and q . The power spectrum (static structure factor) of c-NEFs analyzed elsewhere [5] is then $S(q) = \sum A_N(q)$. In general, the eigenvalues can only be computed numerically. However, in the limit $q \rightarrow 0$, a full analytical investigation is possible by means of power expansions in q , and a clear hierarchy of well-separated Γ_N identified [5]. In that limit, the first term in Eq. (7) dominates, and $f(q \rightarrow 0, t)$ becomes single-exponential in practice. More specifically, from Eqs. (49)-(52) in Ref. [5] one can deduce the decay time due to confinement (c) in the limit of small wave numbers to be:

$$\frac{\tau(\tilde{q} \rightarrow 0)}{\tau_s} \Big|_c = \frac{-1}{\tilde{q}^2 \left(1 - \frac{Ra_s}{Ra_{s,c}}\right)} = \frac{-1}{\tilde{q}^2 \left(1 - \frac{Ra_s}{720}\right)}, \quad (8)$$

where $Ra_{s,c} = 720$ is the critical solutal Rayleigh number at which the convective instability first appears in this model [7]. Hence, the theory predicts a crossover from Eq. (2) (not-including confinement) at large and intermediate q , to the diffusive scaling of Eq. (8) at small q , precisely the kind of behaviour experimentally shown in Fig. 1. We can estimate the wave number q_b corresponding to the minimum decay time by equating Eq. (2) and (8). This gives: $\tilde{q}_b = \sqrt[4]{Ra_{s,c}} = \sqrt[4]{720} \cong 5.2$, in further agreement with the observations in Fig. 1.

For generic q , previous work [5] considered only small (in magnitude) negative solutal Rayleigh numbers. Here we investigate Ra_s values for realistic liquid mixtures, and find different, much richer, $\Gamma_N(q)$ and $A_N(q)$ landscapes, with amplitude crossings not previously observed [5]. In Fig. 2(a) the amplitudes $A_N(\tilde{q})$ of the first three eigenmodes are shown as a function of the dimensionless wave number \tilde{q} , for $Ra_s = -2 \cdot 10^5$. Clearly in different wave number ranges different modes dominate. In particular, the first mode is dominating only for very small and very large wave numbers, while the second one is the leader in the central range $3 \lesssim \tilde{q} \lesssim 30$.

In Fig.2(b) the dimensionless decay times $\tilde{\tau}_N(\tilde{q})$ of the first two eigenvalues are shown as a function of \tilde{q} . Here, one can appreciate that for very large wave numbers all decay times collapse and the time correlation function is nicely approximated by a single exponential decay. At moderate and small wavenumbers, however, the decay time of the first mode is significantly larger than that of the second mode. For very small wave numbers, the first mode dominates in amplitude and a single-exponential decay is again recovered. In the range $0.3 \lesssim \tilde{q} \lesssim 2$, both modes play a significant role and the time correlation

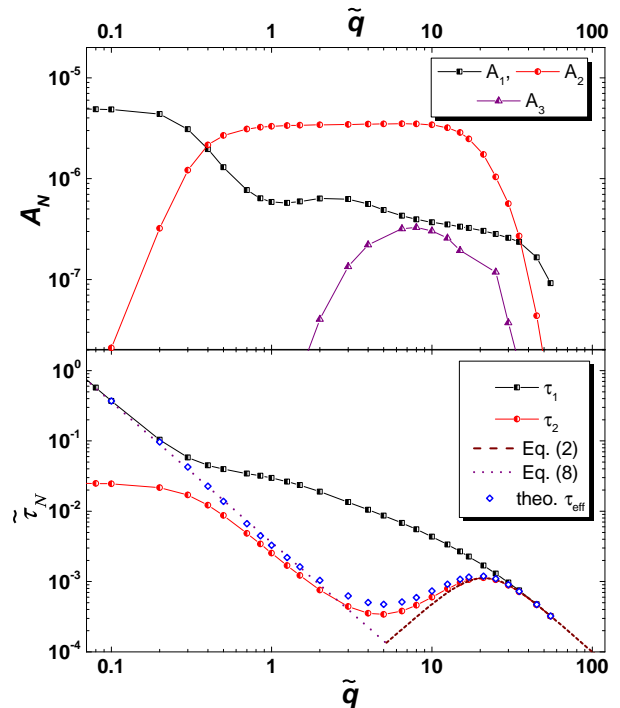


FIG. 2. (color online) (Top) Log-log plot of the amplitude of the first three eigenmodes A_N , for $N = 1, 2, 3$, as a function of the dimensionless wave number q for $Ra_s = -2 \cdot 10^5$. (Bottom) Log-log plot of the dimensionless decay times of the two first eigenvalues $\tau_N = \tau_N/\tau_s$, for $N = 1, 2$ as a function of the dimensionless wave number for the same Ra_s . Eqs.(2),(8) and the theoretical data points reported in Fig.1 are also plotted for direct comparison.

function should show signatures of a double exponential decay. Indeed, all our data (experimental, theoretical and simulations) clearly show such signatures, a detailed analysis of which will be presented in future publications.

Regardless of the multiple exponential character, a single effective decay time $\tau_{\text{eff}}(q)$ can be defined by $f(q, \tau_{\text{eff}}) = 1/e$. In Fig. 1 we show results for theoretical $\tau_{\text{eff}}(q)$, computed via Eq. (7) from the amplitudes and decay rates of Fig. 2. All the features seen in the experimental data points are well-reproduced by the theory. Noticeably the slowing-down observed for small wave numbers is clearly related to confinement, since this is the only ingredient added to the theory that gives Eq. (2). Surprisingly, while confinement has a moderate damping impact on the intensities of c-NEFs [1, 5], it dramatically changes their dynamics, and large-scale c-NEFs are found to decay slower, in agreement with experimental results.

The theory [5] assumes that viscous dissipation dominates, and neglects the effect of fluid inertia; this is justified by the fact that in all liquids momentum diffusion is much faster than mass diffusion, i.e., the Schmidt number $Sc = \nu/D$ is very large. While neglecting inertial

effects is a good approximation at most wavenumbers of interest, it is known that, depending on Ra_s , it fails at sufficiently small wavenumbers due to the appearance of inertial *propagative modes* [26] (closely related to gravity waves) driven by buoyancy. In order to confirm that the slowing down we observe is due to confinement and not inertia we have performed numerical simulations that account for inertial effects and confinement [27, 28], see [25] for details. Data points from a numerical simulation with fluid parameters matching the experimental ones are shown in Fig.1. An excellent agreement is visible for this dataset among experimental, theoretical and simulation results, confirming that inertia effects are not relevant in our experiments. We note, however, that for thicknesses $L \gtrsim 5$ mm, not accessible in the experiments reported here, the simulations do show oscillatory time correlation functions (propagative modes) at the smallest wavenumbers [28].

The effects of confinement are controlled by the solutal Rayleigh number and it is important to further investigate a range of conditions. Experimentally, we study three different Rayleigh numbers in the range $4 \cdot 10^4 \leq |Ra_s| \leq 1.2 \cdot 10^7$ by changing the thickness of the sample in the range $0.7 \leq L \leq 5$ mm. All these experiments were performed on the same tetralin and n-dodecane sample with a constant thermal difference of $\Delta T = 20$ K. In Fig.3, experimental data points are reported as filled symbols for three different Rayleigh numbers, along with results obtained from numerical calculations from the theoretical model and simulations, which are shown as open symbols and open-dotted symbols, respectively. Good agreement is observed between experiments, theory, and simulations for all data points.

We conclude that confinement has a moderate damping impact on the intensities of large-scale non-equilibrium concentration fluctuations, but, in the presence of gravity, it strongly affects their dynamics. Experiments, as well as theory and simulations, show that the slowing down is determined by the solutal Rayleigh number that, in this study, is controlled solely by the confinement distance L . Large-scale fluctuations are confined to evolve in an essentially quasi-two-dimensional manner by the boundaries, and we found them to behave diffusively but with a greatly enhanced diffusion coefficient.

This is in contrast to the case of diffusion in a microgravity environment where the coupling to velocity fluctuations greatly enhances the intensity of the c-NEFs but does not alter their Fickian diffusive dynamics [29]. In strongly confined systems, such as porous media, the buoyancy driven acceleration of the fluctuations is eliminated by confinement already at mesoscopic scales. In the absence of confinement, however, the gravitational acceleration is eventually suppressed by inertial effects leading to propagative modes; confinement is expected to also strongly affect the dynamics of these gravity waves, as we will explore in future work.

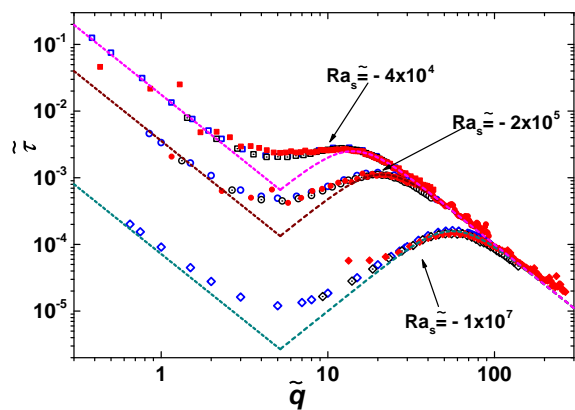


FIG. 3. (color online) Dimensionless decay times for different solutal Rayleigh numbers: Log-log plot of the dimensionless decay times τ as a function of dimensionless wave number q for different Rayleigh numbers. Filled red markers are experimental data, open blue are for calculations based on the FHD model, and open-dotted black are from numerical simulations. Data for three different Rayleigh numbers are shown: squares for $Ra_s = -4 \cdot 10^4$, circles for $-2 \cdot 10^5$ and diamonds for $-1 \cdot 10^7$.

Interestingly, we find that the dimensionless wave number identifying where confinement coexists with gravity is related to the critical solutal Rayleigh number $Ra_{s,c} = 720$ where the convective instability first appears [7]. This is a signature of the Onsager regression hypothesis stating that the dynamics of the fluctuations contains all of the signatures seen in the deterministic dynamics, which is known to be controlled by the Rayleigh number. Our work indicates that the study of the dynamics, rather than the intensity of non-equilibrium fluctuations, gives deep insights into the competition of physical processes such as diffusion, buoyancy, and confinement.

J.M.O.d.Z. acknowledges support from the UCM/Santander Research Grant PR6/13-18867 during a sabbatical leave at Anglet, when part of this work was developed. F.C. acknowledges fruitful discussions with Alberto Vailati and Roberto Cerbino. A.D. was supported in part by the U.S. National Science Foundation under grant DMS-1115341 and the Office of Science of the U.S. Department of Energy through Early Career award number DE-SC0008271.

Correspondence and requests for materials should be addressed to F.C. (fabrizio.croccolo@univ-pau.fr)

-
- [1] J. M. Ortiz de Zárate and J. V. Sengers, *Hydrodynamic fluctuations in fluids and fluid mixtures* (Elsevier, Amsterdam, 2006).
 - [2] J. V. Sengers and J. M. H. L. Sengers, *Annu. Rev. Phys. Chem.* **37**, 189 (1986).

- [3] A. Vailati and M. Giglio, *Nature* **390**, 262 (1997).
- [4] A. Vailati and M. Giglio, *Phys. Rev. E* **58**, 4361 (1998).
- [5] J. M. Ortiz de Zárate, J. A. Fornés and J. V. Sengers, *Phys. Rev. E* **74**, 46305 (2006).
- [6] F. Croccolo, D. Brogioli, A. Vailati, M. Giglio and D. S. Cannell, *Phys. Rev. E* **76**, 041112 (2007).
- [7] A. Ryskin, H. W. Müller, and H. Pleiner, *Phys. Rev. E* **67**, 046302 (2003).
- [8] F. Croccolo, H. Bataller, and F. Scheffold, *J. Chem. Phys.* **137**, 234202 (2012).
- [9] P. N. Segrè, R. Schmitz and J. V. Sengers, *Physica A* **195**, 31 (1993).
- [10] P. N. Segrè, and J. V. Sengers, *Physica A* **198**, 46 (1993).
- [11] F. Croccolo, D. Brogioli, A. Vailati, M. Giglio and D. S. Cannell, *App. Opt.* **45**, 2166 (2006).
- [12] F. Croccolo, PhD thesis, Milano (2006).
- [13] F. Croccolo, H. Bataller, and F. Scheffold, *Eur. Phys. J. E*, in press.
- [14] F. Croccolo, F. Scheffold and A. Vailati, *Phys. Rev. Lett.* **111**, 014502 (2013).
- [15] C. Soret, *Arch. Sci. Phys. Nat.* **3**, 48 (1879).
- [16] S. R. de Groot and P. Mazur, *Nonequilibrium thermodynamics* (North-Holland, Amsterdam, 1962).
- [17] G. S. Settles, *Schlieren and Shadowgraph Techniques* (Springer, Berlin, 2001).
- [18] S. Trainoff, and D. S. Cannell, *Phys. Fluids* **14**, 1340 (2002).
- [19] F. Croccolo, and D. Brogioli, *App. Opt.* **50**, 3419–3427 (2011).
- [20] The probing beam is a plane parallel beam of quasi-monochromatic light as in previous setups [8, 14]. After the sample no collecting lens is used. A Charged Coupled Device sensor (IDS, UI-6280SE-M-GL) with a resolution of 2448×2048 pixels of $3.45 \times 3.45 \mu m^2$ is placed at a distance of $z = (100 \pm 10)$ mm from the detector. Images are cropped to square resolution of 2048×2048 pixels. In this arrangement the size of the image is dictated by the real size of the CCD sensor, which is 7.066 mm. This fixes the minimum wave vector to $q_{\min} = 8.89 \text{ cm}^{-1}$.
- [21] R. Cerbino, and V. Trappe, *Phys. Rev. Lett.* **100**, 188102 (2008).
- [22] G. Cerchiari, F. Croccolo, F. Cardinaux, and F. Scheffold, *Rev. Sci. Instrum.* **83**, 106101 (2012).
- [23] $\rho = 0.8407 \text{ g cm}^{-3}$, $D = 6.21 \times 10^{-6} \text{ cm}^2 \text{ s}^{-1}$, $\nu = 1.78 \times 10^{-2} \text{ cm}^2 \text{ s}^{-1}$, $S_T = 9.5 \times 10^{-3} \text{ K}^{-1}$, $\beta_T = 9.23 \times 10^{-4} \text{ K}^{-1}$, $\beta_s = 0.27$, $\psi = c_o(1 - c_o)S_T\beta_s/\beta_T = 0.695$ from [24] and references therein.
- [24] J. K. Platten, M. M. Bou-Ali, P. Costesèque, J. F. Dutrieux, W. Köhler, C. Leppla, S. Wiegand, and G. Wittko, *Phil. Mag.* **83**, 1965 (2003).
- [25] See Supplemental Material at [URL will be inserted by publisher] for further details on the theoretical calculations, the numerical simulations, and an empirical fit to the data.
- [26] C. J. Takacs, G. Nikolaenko and D. S. Cannell, *Phys. Fluids* **100**, 234502 (2008).
- [27] F. Balboa Usabiaga, J. B. Bell, R. Delgado-Buscalioni, A. Donev, T. G. Fai, B. E. Griffith, and C. S. Peskin, *SIAM J. Multiscale Model. Simul.* **10**, 1369 (2012).
- [28] S. Delong, Y. Sun, B.E. Griffith, E. Vanden-Eijnden and A. Donev, submitted, <http://arxiv.org/abs/1410.0240>.
- [29] A. Vailati, R. Cerbino, S. Mazzoni, C. J. Takacs, D. S. Cannell and M. Giglio, *Nature Comm.* **2**, 290 (2011).

Supplemental material for: Slowing-down of non-equilibrium concentration fluctuations in confinement.

Cédric Giraudet¹, Henri Bataller¹, Yifei Sun², Aleksandar Donev², José Maria Ortiz de Zárate³ and Fabrizio Crococo¹

¹*Laboratoire des Fluides Complexes et leurs Réservoirs,*

Université de Pau et des Pays de l'Adour, 64600 Anglet, France

²*Courant Institute of Mathematical Sciences, New York University, New York, NY 10012, USA and*

³*Departamento de Física Aplicada I, Universidad Complutense, 28040 Madrid, Spain*

(Dated: October 27, 2022)

FLUCTUATING HYDRODYNAMICS

Thermal fluctuations in non-equilibrium systems can be described with the method of fluctuating hydrodynamics (FHD) [1]. For the purpose of this letter, we consider the FHD equations of a binary mixture in the presence of a stationary concentration gradient and in the limit of large Lewis number [2, 3] and large Schmidt number [4]. This approximation is adequate for liquid mixtures (but not for gases) of positive separation ratio [5] and, in the presence of gravity, for sufficiently large wave vectors. By linearizing the complete hydrodynamics equations to leading order in the fluctuations one obtains for the small fluctuations around the steady state [2]:

$$0 = \nabla^4 \delta v_z - \beta_s g (\partial_x^2 + \partial_y^2) \delta c + \frac{1}{\rho} \{ \nabla \times \nabla \times (\nabla \cdot \Pi) \}_z$$

$$\partial_t (\delta t) = D \nabla^2 (\delta c) - (\nabla c) \delta v_z, \quad (S1)$$

where δv_z are the fluctuations in the fluid velocity component along the direction of the gradient, $\nabla c = \nabla c \cdot \hat{z}$, and δc is the mass concentration fluctuations. In Eqs. (S1), in accordance to the general guidelines of FHD, we added a white-noise stochastic momentum flux, $\Pi(\mathbf{r}, t)$, whose statistical properties are given by the fluctuation-dissipation theorem [1, 2]. All other symbols are defined after Eq. (1) of the main text.

The problem of FHD is to solve Eqs. (S1) so as to obtain the correlation function of concentration fluctuations (proportional to the measured ISF [1, 6]) from the correlation function of the stochastic noise $\Pi(\mathbf{r}, t)$. If one does not consider boundary conditions for the fluctuating fields, Eqs. (S1) are readily solved in the Fourier domain [7, 8], leading to a single exponential decay of the ISF with dimensionless decay time given by Eq. (2) of the main text. This solution without boundary conditions is only meaningful for negative Ra_s . To account for confinement effects, one has to implement realistic boundary conditions:

$$0 = \delta v_z = \partial_z \delta v_z = \partial_z \delta c \quad \text{at} \quad z = 0 \text{ and } z = L. \quad (S2)$$

The linear stability of the problem given by Eqs. (S1)-(S2) was studied by Ryskin *et al.* [9] who showed that the quiescent state is stable below a convection threshold: $Ra_s < Ra_{s,c} = +720$.

In a previous publication of theoretical nature [2], it was shown how conditions (S2) can indeed be implemented in FHD by expanding the solution of Eqs. (S1) in a series of hydrodynamic modes that solve an associated eigenvalue problem. The hydrodynamic modes (eigenfunctions) have single decay times $\tau_N(q)$ that are obtained by numerically solving an algebraic equation (Eq.(43) in Ref.[2]). Although all the data reported in this letter are for negative Ra_s , we note that the solution to Eqs. (S1) incorporating the boundary conditions (S2) is meaningful for any $Ra_s < +720$, including the whole range of positive solutal Rayleigh numbers below the convection threshold [2, 9].

The focus of [2] was on the static structure factor $S(q)$ of c-NEFs and the dynamics, although implicitly included, was not investigated. In this work we focus on the dynamics, and obtain Eqs. (7) and (8) of the main text. In addition, we numerically evaluate the decay times $\tau_N(q)$ and corresponding amplitudes $A_N(q)$ for a range of previously unexplored large negative values of the solutal Rayleigh number relevant to the experimental conditions. The results of these calculations are summarized in Fig. 2 of the main text. From the data contained in this figure, using Eq. (7), we computed theoretical ISFs that, depending on the wave number q , exhibit a clear multi-exponential behaviour that will be discussed more in detail in future publications. A well-defined effective decay time τ_{eff} can be extracted by evaluating the time the ISF takes to decay to $1/e$. Those theoretical decay times are displayed in Figs. 1 and 3 as open blue symbols, and compared with experiments and simulations.

NUMERICAL SIMULATIONS

We perform computer simulations of the experimental setup using finite-volume methods for fluctuating hydrodynamics described in more detail elsewhere [4, 10, 11]; here we summarize some key points. The numerical methods have been implemented in the IBAMR software framework [12]. The numerical codes solve the following stochastic partial differential equations for the fluctuating velocity field $\mathbf{v}(\mathbf{r}, t)$ and mass concentration $c(\mathbf{r}, t)$ in

a binary liquid mixture [1],

$$\rho \partial_t \mathbf{v} + \nabla p = \eta \nabla^2 \mathbf{v} + \nabla \cdot \Pi - \rho \beta_s c \mathbf{g} \quad (\text{S3})$$

$$\nabla \cdot \mathbf{v} = 0$$

$$\partial_t(c) + \mathbf{v} \cdot \nabla c = D \nabla^2 c, \quad (\text{S4})$$

where $\eta = \rho\nu$ is the shear viscosity, $p(\mathbf{r}, t)$ the pressure and, as in Eqs. (S1), $\Pi(\mathbf{r}, t)$ denotes a white-noise stochastic momentum flux due to thermal fluctuations. Nonlinear advective terms in the velocity equation are neglected in a small Reynolds number approximation. Temperature fluctuations are not considered in a large Lewis number (very fast temperature dynamics) approximation [2]. We assume that the applied temperature gradient ∇T is weak and approximate $T \approx T_o = 298$ K. Note that in (S4), as well as in (S1), we have ignored thermal fluctuations in the mass flux, which are responsible for equilibrium fluctuations in the concentration. This is because our focus is on the much larger non-equilibrium fluctuations induced by the coupling to the velocity equation via the advective term $\mathbf{v} \cdot \nabla c$.

In linearized FHD the equations (S3)-(S4) are expanded to leading order in the magnitude of the fluctuations $\delta c = c - \langle c \rangle$ and $\delta \mathbf{v} = \mathbf{v} - \langle \mathbf{v} \rangle$ around the steady state solution of the deterministic equations [2]. Typical liquid mixtures have a large Schmidt number, $Sc = \nu/D \gg 1$, and under certain conditions one can take a limit of equations (S3)-(S4) as $Sc \rightarrow \infty$; in the linearized setting this over-damped limit amounts to deleting the inertial term $\rho \partial_t \mathbf{v}$ in the velocity equation (S3), [2, 3, 9, 11]. With these simplifications only the component of the velocity parallel to the macroscopic concentration gradient couples to the concentration equations, and after taking a double curl of the velocity equation one obtains equations (S1), [2]. Our numerical method, however, solves the complete hydrodynamic equations (S3)-(S4) in two dimensions with the concentration gradient along the y axis; for this problem there is no difference between two and three-dimensional simulations due to the symmetries of the problem.

With a simple modification of the time-integration algorithm used in the numerical method we can perform simulations with or without the $\rho \partial_t \mathbf{v}$ term in the velocity equation (S3), allowing us to study the importance of fluid inertia [11]. In the inertia-less limit we have confirmed that numerical simulations reproduce the results of the theoretical calculations (see previous section on FHD) based on solving (S1)-(S2) analytically. In the simulations with inertia we have confirmed that, for the range of Ra_s probed experimentally, propagative modes appear only for the largest $Ra_s = 10^7$ but at wavenumbers $q \lesssim 10 \text{ cm}^{-1}$ not resolved in the experiments. For the wavenumbers and Rayleigh numbers experimentally studied, simulations show negligible effects of inertia on the correlation functions, and the same slow decay at long times is observed for confined fluctuations with or

without fluid inertia. Hence, the observed slowing-down is due to confinement only.

In our simulations, the domain is periodic along the x direction. At the top and bottom boundaries, $y = 0, L$, a no-flux boundary condition is imposed for the concentration, $\nabla c = -c_o(1 - c_o)S_T \nabla T$, where $c_o = 0.5$ is the average concentration, and a no-slip boundary condition is imposed for velocity. For comparison, we have also performed simulations employing free-slip boundary conditions for the velocity; these show a qualitatively similar behaviour to the results reported here but differ quantitatively indicating the importance of the boundary conditions (confinement).

The experimentally observed light intensity, once corrected for the optical transfer function of the equipment, is proportional to the intensity of the fluctuations in the concentration averaged along the gradient [1, 2, 13],

$$\delta c_{\perp}(x; t) = \frac{1}{L} \int_0^L \delta c(x, y; t) dy. \quad (\text{S5})$$

The main quantity of interest in our simulations is the Fourier transform $\delta \hat{c}_{\perp}(q; t)$ of the vertically averaged concentration, the time-correlation of which gives the dynamic structure factor appearing in Eq. (7) of the main text:

$$S(q, t) = \langle \delta \hat{c}_{\perp}(q, t) \delta \hat{c}_{\perp}^*(q, 0) \rangle. \quad (\text{S6})$$

After suitable normalization and background subtraction $S(q, t)$ is directly related to the experimental ISF, see Eq. (6) of the main text. We obtain the relaxation time τ from the simulation results by fitting $S(q, t)$ to a sum of two exponentials and solving $S(q, \tau) = S(q, 0)/e$.

The physical parameters used in the simulations are the same as reported in Ref. [23] of the main text and the temperature difference across the sample is $\Delta T = 20$ K, heating from the top boundary. The length of the simulation box in the periodic direction (perpendicular to the gradient) is 6.13 mm. The time step size is sufficiently small to resolve the fast viscous dynamics, $\Delta t = 5 \times 10^{-3}$ s. We skip the initial 1250 seconds (in physical time) of the run to allow the steady state to develop, and then collect data for another 6250 seconds. Different sizes of uniform grids were used for the different sample thicknesses, as summarized in the following table:

Thickness, L	Ra_s	grid resolution
0.7mm	$4 \cdot 10^4$	280×32
1.3mm	$2 \cdot 10^5$	300×64
5mm	$1 \cdot 10^7$	156×128

**PHENOMENOLOGICAL EQUATION FOR THE
DECAY TIMES INCLUDING: DIFFUSION,
GRAVITY AND CONFINEMENT**

We now focus on the shape of the dimensionless decay time $\tilde{\tau}$ as a function of \tilde{q} , with the goal of obtaining an empirical relation to replace Eq. (2) of the main text and incorporate the confinement as described by Eq. (8) of the main text for small wave numbers. Specifically, we propose a phenomenological equation that crosses over analytically from Eq. (8) of the main text at extremely small \tilde{q} to Eq. (2) of the main text at intermediate \tilde{q} , and is therefore useful for a rapid analysis of experimental results. We first notice that the only difference between the two aforementioned equations is that the \tilde{q}^4 term of Eq. (2) becomes 720 in Eq. (8), so we substitute these terms by $720(1 + \tilde{q}^4/720)$, to obtain the empirical equation:

$$\begin{aligned} \left. \frac{\tau(\tilde{q})}{\tau_s} \right|_{d+g+c} &= \frac{1}{\tilde{q}^2 \left[1 - \frac{Ra_s}{720(1 + \frac{\tilde{q}^4}{720})} \right]} = \\ &= \frac{720 + \tilde{q}^4}{\tilde{q}^2 (-Ra_s + 720 + \tilde{q}^4)}, \end{aligned} \quad (S7)$$

which is also plotted in Fig. 1. Clearly a discrepancy is present between Eq. (S7) and the data points for wave vectors around $q_b = 5.18$. The gap can be filled-in by slightly modifying Eq. (S7), adding a term of the second order in \tilde{q} in the numerator:

$$\left. \frac{\tau(\tilde{q})}{\tau_s} \right|_{d+g+c} = \frac{720 + \alpha\tilde{q}^2 + \tilde{q}^4}{\tilde{q}^2 (-Ra_s + 720 + \tilde{q}^4)}, \quad (S8)$$

which does not modify the asymptotic behaviours at large and small \tilde{q} . We find that Eq. (S8) can be used in practice to fit the experimental data points with the

ad hoc constant α as a free parameter. The need for this fill-in procedure can be understood if one notes that the data points are actually effective decay times, obtained by taking the time needed to the correlation function to relax to its $1/e$ initial value, and thus do not have a clear physical interpretation, as do the decay times of the individual eigenmodes.

-
- [1] J. M. Ortiz de Zárate and J. V. Sengers, *Hydrodynamic fluctuations in fluids and fluid mixtures* (Elsevier, Amsterdam, 2006).
 - [2] J. M. Ortiz de Zárate, J. A. Fornés and J. V. Sengers, *Phys. Rev. E* **74**, 46305 (2006).
 - [3] M. G. Velarde and R. S. Schechter, *Phys. Fluids* **15**, 1707 (1972).
 - [4] A. Donev, T. G. Fai, and E. Vanden-Eijnden, *J. Stat. Mech.* P04004 (2014).
 - [5] For mixtures of negative separation ratio, the coupling with temperature fluctuations should not be neglected in the FHD equations [2, 3].
 - [6] F. Croccolo, H. Bataller, and F. Scheffold, *J. Chem. Phys.* **137**, 234202 (2012).
 - [7] P. N. Segrè, R. Schmitz and J. V. Sengers, *Physica A* **195**, 31 (1993).
 - [8] P. N. Segrè, and J. V. Sengers, *Physica A* **198**, 46 (1993).
 - [9] A. Ryskin, H. W. Müller, and H. Pleiner, *Phys. Rev. E* **67**, 046302 (2003).
 - [10] F. Balboa Usabiaga, J. B. Bell, R. Delgado-Buscalioni, A. Donev, T. G. Fai, B. E. Griffith, and C. S. Peskin, *SIAM J. Multiscale Model. Simul.* **10**, 1369 (2012).
 - [11] S. Delong, Y. Sun, B.E. Griffith, E. Vanden-Eijnden and A. Donev, submitted, <http://arxiv.org/abs/1410.0240>.
 - [12] B. E. Griffith, R. D. Hornung, D. M. McQueen and C. S. Peskin, *J. Comput. Phys.* **223**, 10 (2007). Software available at <http://ibamr.googlecode.com>
 - [13] S. Trainoff, and D. S. Cannell, *Phys. Fluids* **14**, 1340 (2002).